Journal of Power Sources 190 (2009) 173–183

Contents lists available at ScienceDirect

Journal of Power Sources

journal homepage: www.elsevier.com/locate/jpowsour

Micro-hybrid electric vehicle application of valve-regulated lead–acid batteries in absorbent glass mat technology: Testing a partial-state-of-charge operation strategy

S. Schaeck*, A.O. Stoermer, E. Hockgeiger

BMW Group, Powertrain Development, Energy Storage, Hufelandstrasse 4, 80788 München, Germany

ARTICLE INFO

Article history:
Received 9 June 2008
Received in revised form 10 October 2008
Accepted 14 October 2008
Available online 1 November 2008

Keywords:
Valve-regulated lead–acid battery (AGM)
Micro-hybrid electric vehicle
Energy management
Operating strategy
Field data analysis
Charge acceptance

ABSTRACT

The BMW Group has launched two micro-hybrid functions in high volume models in order to contribute to reduction of fuel consumption in modern passenger cars. Both the brake energy regeneration (BER) and the auto-start-stop function (ASSF) are based on the conventional 14 V vehicle electrical system and current series components with only little modifications. An intelligent control algorithm of the alternator enables recuperative charging in braking and coasting phases, known as BER. By switching off the internal combustion engine at a vehicle standstill the idling fuel consumption is effectively reduced by ASSF. By reason of economy and package a lead–acid battery is used as electrochemical energy storage device.

The BMW Group assembles valve-regulated lead–acid (VRLA) batteries in absorbent glass mat (AGM) technology in the micro-hybrid electrical power system since special challenges arise for the batteries. By field data analysis a lower average state-of-charge (SOC) due to partial state-of-charge (PSOC) operation and a higher cycling rate due to BER and ASSF are confirmed in this article.

Similar to a design of experiment (DOE) like method we present a long-term lab investigation. Two types of 90 Ah VRLA AGM batteries are operated with a test bench profile that simulates the micro-hybrid vehicle electrical system under varying conditions. The main attention of this lab testing is focused on capacity loss and charge acceptance over cycle life. These effects are put into context with periodically refresh charging the batteries in order to prevent accelerated battery aging due to hard sulfation. We demonstrate the positive effect of refresh chargings concerning preservation of battery charge acceptance. Furthermore, we observe moderate capacity loss over 90 full cycles both at 25 °C and at 3 °C battery temperature.

1. Introduction: BMW EfficientDynamics

Within the BMW EfficientDynamics initiative several activities are focused on the reduction of fuel consumption and CO_2 emissions of modern passenger cars. Those developments are based on increased efficiency of the internal combustion engines (ICE), a consequent lightweight construction strategy and sophisticated aerodynamic features of the car body. By an intelligent energy management the vehicle electrical power system also contributes to the EfficientDynamics program resulting in an upgrade of the conventional power supply to the micro-hybrid electrical power system. The BMW short-term strategic approach is to implement micro-hybrid functionality in almost the whole product portfolio in order to reduce the average CO_2 emissions of the BMW vehicle fleet according to the ACEA (European Automobile Manufacturers' Association) voluntary agreement in 1998. In a further mid-term oriented step higher levels of powertrain hybridization are developed and implemented in mild and full-hybrid vehicles.

2. Micro-hybrid electrical power system

As first Original Equipment Manufacturer (OEM) the BMW Group has introduced micro-hybrid functions in high volume series vehicles in March 2007 (see Fig. 1). As described in detail in Sections 2.2 and 2.3 the micro-hybrid functions are based on the 14 V power system with only slightly modified current series components and a 12 V valve-regulated lead–acid (VRLA) battery in absorbent glass mat (AGM) technology.

Diegelmann et al. [1] describe the micro-hybrid electric vehicle (Micro-HEV) as an intermediate stage towards the development of BMW mild-hybrid electric vehicles (Mild-HEV) and full-hybrid electric vehicles (Full-HEV). The lowest level of hybridization, the Micro-HEV, combines brake energy regeneration (BER) with an auto-start-stop function (ASSF) of the internal combustion engine,

* Corresponding author. Tel.: +49 89 382 78653; fax: +49 89 382 42827.
E-mail address: stefan.schaeck@bmw.de (S. Schaeck).

0378-7753/$ – see front matter © 2008 Elsevier B.V. All rights reserved.
doi:10.1016/j.jpowsour.2008.10.061

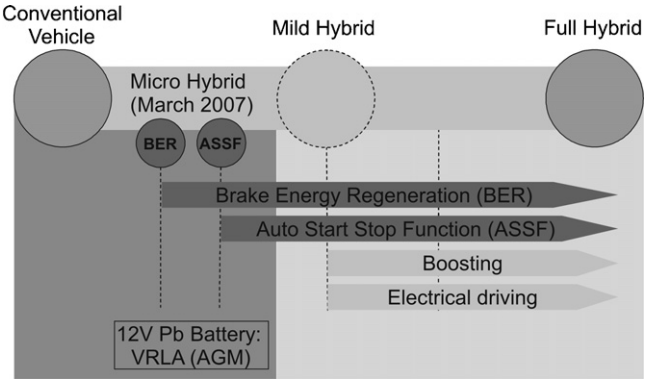

Fig. 1. According to [1]. Powertrain micro-hybridization is described as intermediate stage towards BMW mild-hybrid and full-hybrid electric vehicles.

which is conceptually part of higher level HEVs as well. Advanced functionalities like boosting and electrical driving require higher voltage systems and therefore nickel/metal-hydride (NiMH) and high-power lithium-ion (Li-ion) batteries, respectively. More specific vehicle attributes of Mild-HEVs and Full-HEVs, especially energy management aspects and energy storage requirements are discussed by Karden et al. [2].

2.1. Topology of the Micro-HEV power system

In Fig. 2 the topology of the micro-hybrid electrical power system is schematically depicted. The intelligent battery sensor (IBS) acts as a main component in conjunction with a bit-serial data (BSD) interface, which is an advanced interface to the slightly modified alternator. The IBS is directly connected to the negative terminal post of the VRLA battery. By continuously measuring battery voltage, current and temperature also in the sleep mode, the intelligent battery sensor acquires critical data for the algorithms of brake energy regeneration and automatic engine start/stop. These algorithms are implemented in the power management software module as part of the vehicle electrical energy management on the engine control unit (ECU). The ECU and the electric consumers within the vehicle electrical system are cross-linked via bi-directional communication in a conventional controller area network (CAN) bus.

2.2. Functionality of automatic engine start/stop

The auto-start-stop function, ASSF, switches off the internal combustion engine automatically if a standing phase is recognized—like stopping at a traffic light, in a traffic jam or at a railroad crossing. ASSF restarts the engine automatically on demand of the driver. For the driver the operation of ASSF is implemented as intuitional as possible. Fig. 3 illustrates the procedure of ASSF in combination with a manual gear shift. The ASSF is only triggered if the driver stops the car, engages the neutral gear and releases the clutch. If several technical on-board requirements are fulfilled, ASSF will switch off the engine automatically and display the current state of the machine in the instrument panel.

Approximately the amount of fuel which is usually consumed by the engine idle during the red traffic light phase is not used and the according CO_2 emissions are not produced. If the driver operates the clutch and therefore sets the requirement for continuation of the ride, the engine will be restarted automatically. The high number of starts has to be accomplished reliably, accompanied by as few vibrations and noise as possible. Furthermore, the traction power has to be provided immediately after an engine switch-on. Therefore, the starter system is enforced compared to previous series systems.

During the vehicle standstill all electrical consumers are provided with electrical energy from the battery acting as additional load for the battery. The engine restart after each automatic stop also results in a significantly increased number of high-rate load phases during battery cycle life. These aspects will be faced in Section 3.

The automatic restart opposes the fuel saving potential during standstill by temporarily increased consumption. This effect is compensated by a minimum engine-off time period of 5 s according to Wolff et al. [3]. They report about a maximum potential for fuel savings of 3.5% in the New European Driving Cycle (NEDC). In the first launch, ASSF is integrated in 4-cylinder vehicles with manual gear shift and always combined with BER. Since BER is available in vehicles with automatic transmission and/or bigger engines without ASSF, the number of affected cars is higher.

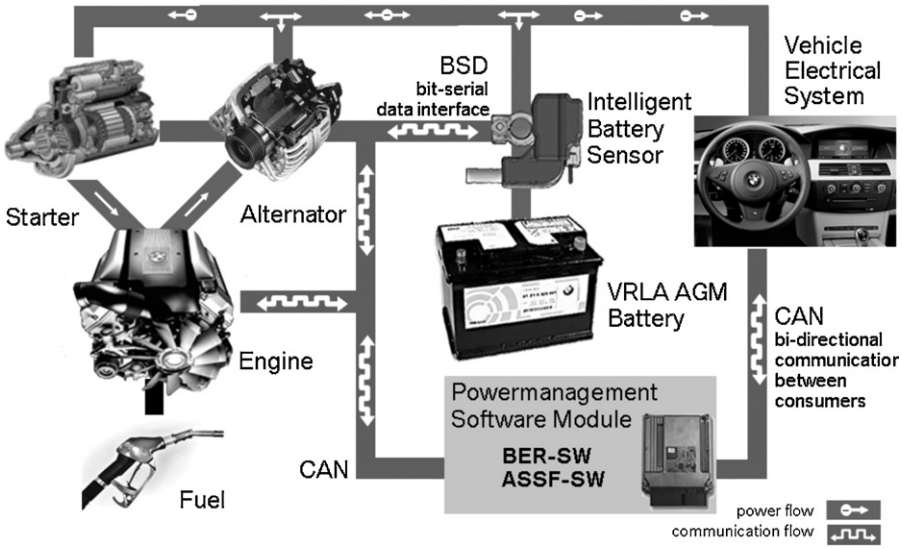

Fig. 2. Schematic topology of the micro-hybrid electrical power system. Main components are the power management software (SW) module integrated in the engine control unit, the VRLA AGM battery and the intelligent battery sensor.

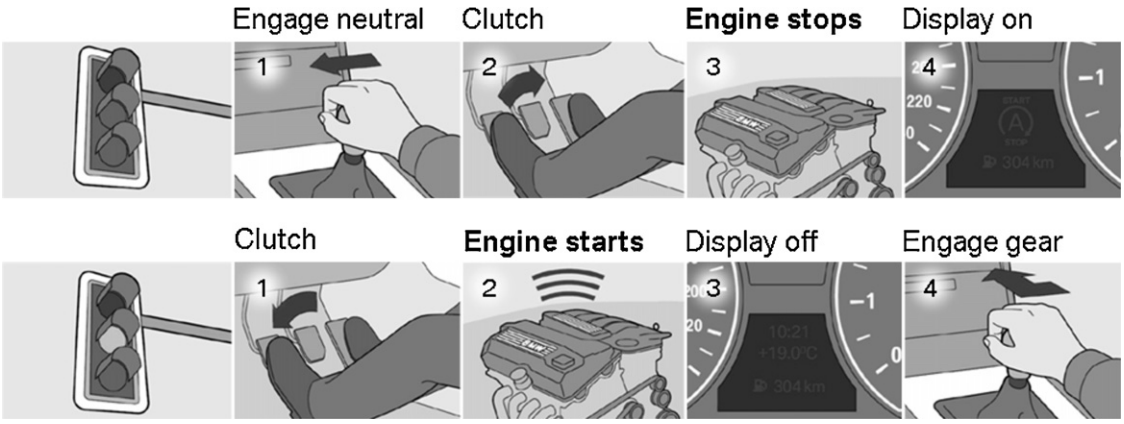

Fig. 3. According to [1]. Sequences of an automatic engine stop and start with ASSF. The driver induces automatic engine stops and starts by properly handling the gear shift and the clutch.

2.3. Functionality of brake energy regeneration

In the conventional electrical system, the power supply requirements during common driving phases are covered by the alternator as only supplier. In Fig. 4 this is labelled as conventional charging. So far, the alternator charge regulator was not directly linked to specific driving phases like traction or coasting/breaking mode. Therefore, the electrical energy was converted independently of the state of the machine. The intelligent alternator algorithm of the BER function realizes the possibility to partly regenerate the brake energy of the vehicle, known as recuperation.

The energy reservoir for brake energy regeneration is the kinetic energy of the vehicle in coasting and braking phases. In this mode, the moment of inertia drives the engine with engaged gear. Therefore, the rotational speed of the alternator is not powered by fuel consumption, but by the vehicle inertia moment, i.e. the already 'paid' energy. By increasing the exciting current of the rotator magnetic field the retarding force of the ICE is slightly raised as well. The BER software controls the rotator exciting current to an alternator output of 14.8 V on-board voltage. This implicates over-covering of the electrical consumers resulting in recuperative charging of the battery (cf. Fig. 4).

The conversion of mechanical to electrical energy strongly depends on the charge acceptance of the battery at the moment of the voltage increase. As the charge acceptance is inversely proportional to the state-of-charge (SOC) for all types of lead–acid batteries, the state-of-charge has to be regulated to a certain level below 100% SOC while driving. This regime of BER, labelled as charge sustainment in Fig. 4, actually enables the partial state-of-charge (PSOC) operation of the battery. Allowing for the demand of load current of electrical consumers, the alternator output voltage is controlled to the battery voltage. Thus, the alternator control system accomplishes approximately zero discharging/charging of the battery while driving, in order to keep it at partial state-of-charge. The intelligent alternator algorithm triggers this charge sustainment regime only if the SOC is within a certain range, ≈79–85% SOC, in the first implementation of BER.

If at some point the upper SOC level is reached, the vehicle electrical system is supplied with electrical energy from the battery. Then, the raised state-of-charge, which was ideally charged by recuperative braking before, is reduced. In this active discharge regime (see Fig. 4) the alternator generates less electrical power resulting in a decreased power demand on the internal combustion engine.

In the New European Driving Cycle, the decreased power demand of the alternator in the active discharge regime amounts to a potential of up to 3% reduction of fuel consumption compared to cars without BER. Actually, as with ASSF, the total fuel saving potential depends on the chronology of the driving phases, the storage capacity for the regeneratable energy and, especially, the charge acceptance of the lead–acid battery [4,5]. These aspects and

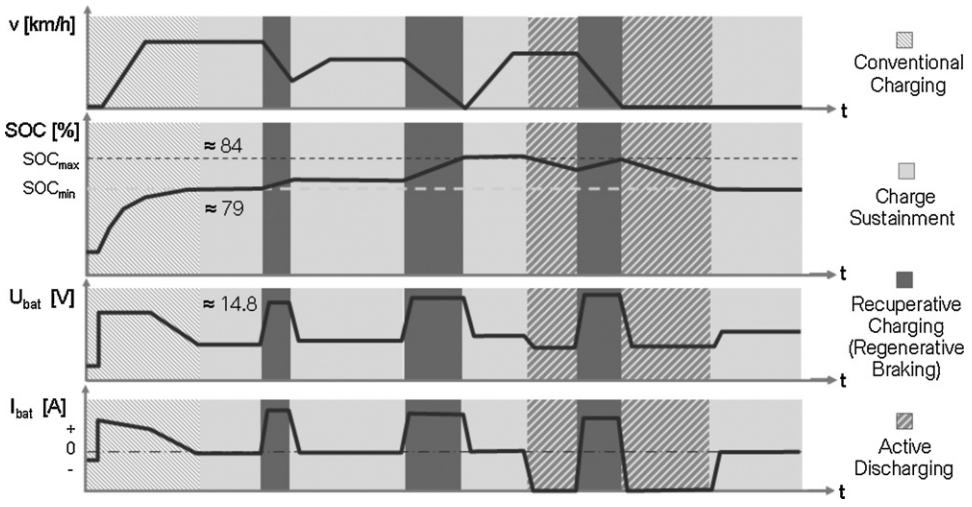

Fig. 4. The sequence of battery voltage, current and SOC depending on an exemplary driving pattern with BER at a glance.

the possibly modified reliability of the batteries regarding aging mechanisms gave rise to the long-term lab investigation of PSOC operation described in Sections 4 and 5. The bench testing includes a battery refresh function that regularly interrupts BER. Then, a conventional charging period is applied in order to fully charge the battery. It is intended to prevent accelerated battery aging due to hard sulfation during PSOC operation. The battery refresh function is introduced in Section 3.3.

3. Challenges for the battery

The automotive battery faces changed challenges under micro-hybrid application concerning both performance and durability. Thereby, charge acceptance is a key parameter. In the context of micro-hybrid electric vehicles, the term 'charge acceptance' is used in a slightly different way as commonly known [6]. Here, charge acceptance does not mean fast recharging at low temperatures from high depth of discharge (DOD) levels, referred as stationary charge acceptance. Instead, charge acceptance is interpreted as dynamic charge acceptance as introduced by Karden et al. [6] which means that preferably high charge currents are obtained in short boost phases at moderate temperatures—independent of the battery's short-term history. According to Sauer et al. [7] the charge/discharge history of the battery has a not yet understood impact on the dynamic charge acceptance. This is observed by twice as high charge acceptance following a discharge phase instead of a charge phase [7]. In the following sections the charge acceptance is addressed in detail.

The aging behavior is also directly influenced by the operation strategy of the Micro-HEV. In several references, for example [6], the effects of higher cycling rates and PSOC operation in Micro-HEVs are estimated. In the following section we present first data from field analysis of a high number of BMW customer Micro-HEVs that confirm the main expectations on the battery influences. Please note that quantitative statements may strongly depend on the customer behavior and – if the considered number of vehicles is statistically significant – on the specific Micro-HEV operating strategy, of course.

3.1. Field analysis of BMW Micro-HEVs

In the automotive industry the leading OEMs make use of modern business intelligence methods as part of the technical verification processes. In the field, the theoretical amount of technical information on vehicle operation jumps up following start of production. This information can be made accessible provided that data availability and data plausibility are ensured and that efficient data analysis methods are implemented. Thus, various insights of scientific relevance into the operation of vehicles can be acquired. This method of acquisition of technical information is known as continuous after sales analysis.

In brief, the data flow is designed as follows: During vehicle operation by the customer various technical data are logged by the engine control unit and stored in the vehicle info recorder. Parts of the power supply topology like the intelligent battery sensor discussed in Fig. 2 are categorical requirements concerning battery related information. The info recorder is read out in the workshop during the subsequent repair service and selected data are anonymized and automatically transferred to a central server via the worldwide vehicle diagnosis network. The data are retained in data warehouses and the analysis specialists make use of the data with modern data warehouse analysis tools like online analytical processing. The described way of data processing is oriented at the knowledge discovery in databases (KDD) process as introduced in [8,9].

The data illustrated in Fig. 5 is acquired in the described way of data processing. The database is formed by BMW compact and mid-sized cars that were produced after launching brake energy regeneration and automatic engine start/stop in March 2007 and sold in the European market. We are able to compare Micro-HEVs (light circle symbols in Fig. 5a) and corresponding vehicles without micro-hybrid functionality (dark square symbols in Fig. 5a) since BER and ASSF are not yet part of all derivatives. The number of read-out events is comparable as well. It accounts for about 80.000 read-outs in the case of Micro-HEVs and about 60.000 read-outs for the conventional vehicles.

3.1.1. Battery cycling

In Fig. 5a the relative number of read-outs is shown versus battery cycling given as number of full cycles per 1000 km. The number of read-outs is related to the total number of read-outs separately for both groups, resulting in approximately area-normalized curves after spline interpolation. In the case of Micro-HEVs, the distribution shows a slight broadening and a shift of the maximum to higher battery cycling of about 0.5 full cycles per 1000 km mileage. The increased cycling rate directly linked to the functionality of

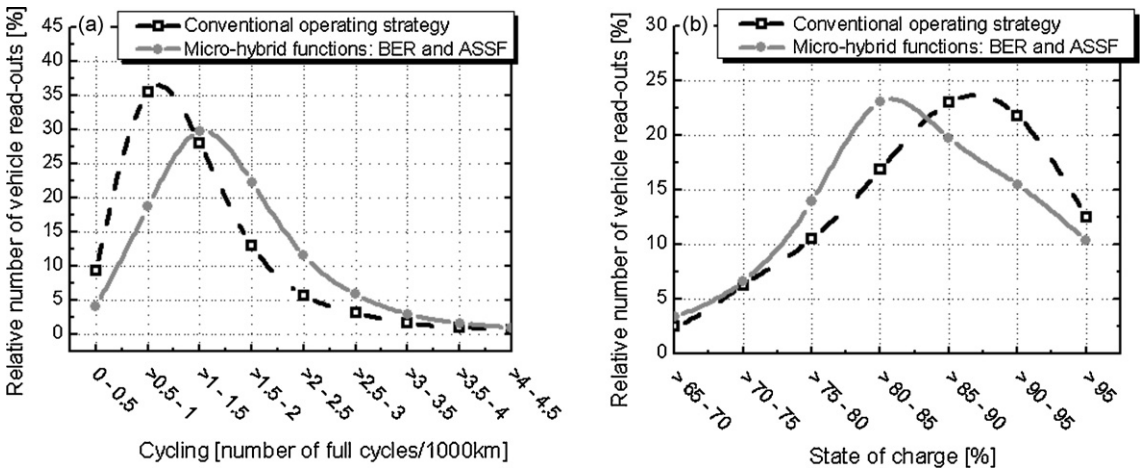

Fig. 5. Field data analysis of BMW compact and mid-sized cars illustrating the higher cycling rate (a) and the lower average SOC (b) of AGM batteries in the micro-hybrid electrical power system.

BER and ASSF as described in Sections 2.2 and 2.3. The broadening might reflect the raised individual influence of the customer on battery cycling as the number of regenerative braking phases and the number of automatic engine stops strongly depends on the driving profile and on the customer's decision to engage the neutral gear, respectively. By integration of the distributions in Fig. 5a we observe a total increase of the average battery cycling rate of 29% in the field due to micro-hybridization. This increase of about 0.35 full cycles per 1000 km results in an accumulated total turnover of 100 full cycles after about 65,000 km in the case of micro-hybrid electric compact and mid-sized cars.

3.1.2. Battery state-of-charge

In Fig. 5b the read-out processes are consulted for a snapshot of the SOC distribution. Again, broadening of the distribution is observed. The maxima of the spline interpolated plots show a difference of about 8% SOC. As described in Section 2.3 one would ideally expect a difference of about 15–20%. However, there are a few reasons for a SOC decrease of moderate 8%. Firstly, also in the conventional power system where the battery is controlled to be fully charged, the maximum is located at about 90–95% SOC. This is mainly due to long vehicle standstills and/or due to deficient covering of the power supply requirements. Secondly, battery monitoring of BER may require higher battery voltage from the alternator although active discharge or zero current regulation is actually encoded (cf. Fig. 4). This feature is deduced from the hierarchic architecture of power supply priorities. For example, safety related electric consumers are allocated highest priority and, therefore, BER, ASSF and other electric functions may work in a fail-safe mode during the power-on time of the highest prioritized consumers. Thirdly, the refresh function is responsible for periodically fully charging the battery in the Micro-HEVs resulting in higher SOC at that time. By integration over all read-outs the total average SOC decrease can be quantified for about 5%. Note that the batteries had a maximum age of about 1 year at the time of after sales analysis. A significant amount is not older than 6 months.

3.2. Functional integration of VRLA AGM batteries

As demonstrated in the previous section the expected service life of flooded batteries (100 full cycles, e.g. [10]) is reached after about 65,000 km. With an assumed average customer mileage of 15,000 km per year this is equivalent to a cycle life of about 4 years. Additionally, the decreased SOC in Micro-HEVs (cf. Fig. 5b) has an accelerating impact on battery aging due to sulfation [11], which will be discussed in Section 5. Due to acid stratification this effect is supposed to have an even pronounced effect on the flooded battery type [12].

Another predicted disadvantage of flooded batteries in micro-hybrid applications is charge acceptance, which is the most critical limiting factor [6] relating energy efficiency of brake energy regeneration. The characteristics of the battery to accept charge current within time periods of about 2–10 s at moderate temperatures independent of the short-term cycling history of the battery is the main criterion of applicability in a Micro-HEV [7]. Karden et al. [6] have demonstrated in a comparative series of measurements that the AGM battery type enables a significant higher dynamic charge acceptance of about 28% on average.

Summarized, there are mainly three reasons to apply AGM batteries in Micro-HEVs: AGM batteries have a better charge acceptance, their reliability regarding cycling is about three times better [10] and they have lower addiction to sulfation. Furthermore, AGM batteries constitute best compromise between performance, package and price. For example, supercaps (also known as ultra-capacitors) are designed as alternative energy storage devices in advanced Micro-HEVs because of their reliability and performance parameters [4]. However, they are not yet mounted due to high prices and low degree of maturity.

3.3. Application of battery refresh charging

The effect of hard sulfation strongly scales with the duration of not recharged lead sulfate especially at the negative plates and at high temperatures [13]. This issue opposes the fundamental idea of PSOC operation since random charge acceptance prerequisites uncharged capacity of the battery. Hard sulfation can cause early battery failure as the transition from reversible to irreversible sulfation may even be negatively assisted by the customer behavior.

In a long-range step, battery manufacturers may focus on optimizing the batteries towards modified requirements, e.g. improvements of the formulae of the (negative) active mass and of the manufacturing parameters. In a short-term application-oriented step, the battery may also be prevented from hard sulfation by on-board operating strategy. This is expected from periodically recharging the battery to 100% SOC in order to shrink or dissolve the grown sulfate crystals especially at the negative plate [13]. Gibson and Peters [14] have investigated the inability of flooded lead–acid batteries to be recharged after inactivity of several weeks. A similar effect is expected also during PSOC operation of AGM batteries [13,15]: Recently formed $PbSO_4$ crystals tend to have a higher dissolution rate in partial cycling operation. This results in a 'recrystallisation' process with irreversible hard sulfation at its end. As a consequence, the lead–acid battery in a Micro-HEV would suffer from accelerated capacity fading and bad charge acceptance with inefficient regenerative braking.

Therefore, a battery refresh function (14.8 V charge voltage) is implemented in the BER software in order to periodically fully charge the battery with respect to a charge factor of about 1.05–1.1. Both the duration of a single battery refresh and the frequency of battery refreshes are dynamically adapted to both the customer behavior and the environmental conditions by the battery power management. Of course, the refresh might reduce the availability of the BER function. On the other hand, decelerated battery aging and better charge acceptance are expected. The actual benefit of applying the battery refresh function in the PSOC operation scheme will be investigated under approximately real conditions in the next sections.

4. Long-term lab investigation of PSOC operation

We present a test procedure similar to a design of experiment (DOE) in this section. It is aimed at the battery behavior under PSOC operation and periodical application of battery refresh cycles. In the first step, the bench test does not include automatic engine stops and starts for practical reasons as the main interest is purely focused on dynamic charge acceptance and refresh efficiency of partially discharged batteries. Therefore, battery cycling that is typical for vehicles solely equipped with BER is performed. In order to evaluate the aging behavior of AGM batteries close to reality but without losing significance, the investigation should be preferably similar to the original system with all relevant parameters to be controllable and observable. For that reason a common vehicle field test might generate interesting phenomenological observations. However, the actual causalities may not be comprehensible as the parameters, which affect battery behavior, are not sufficiently accessible under customer conditions. Thus, the presented investigation is exclusively performed in the lab and based on logged CAN bus data from a BMW prototype Micro-HEV. We use commercial, released automotive batteries (90 Ah VRLA AGM with flat plate

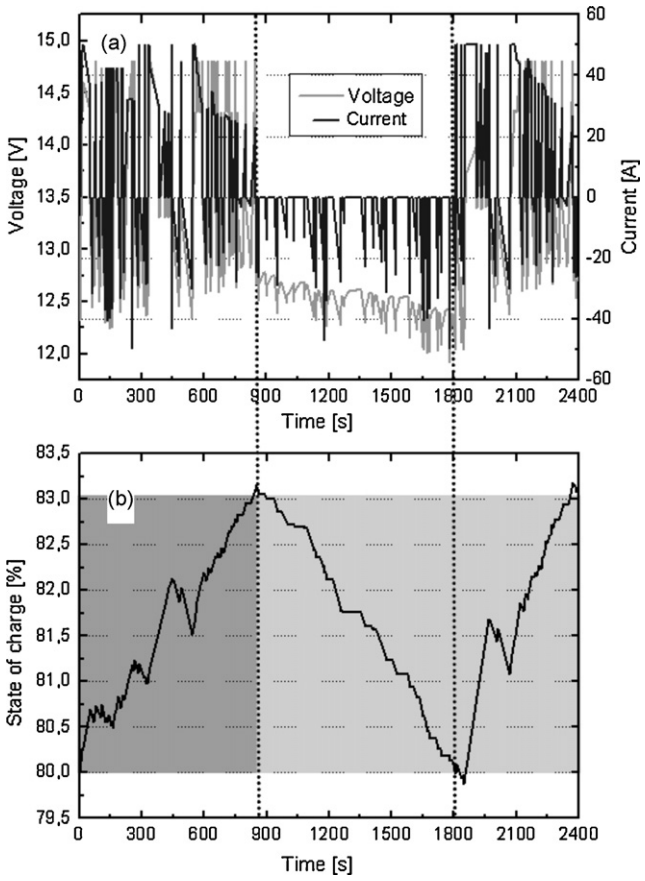

Fig. 6. The *U*/*I*-profile selected from a Micro-HEV prototype was transferred to the lab test bench (a). The resulting characteristic PSOC curve (b) represents the fundamental idea of brake energy regeneration.

design) from leading battery manufacturers without any modifications. The stage of battery development was at the level of early 2006.

4.1. Selection of driving profile

Fig. 6a depicts the chosen voltage/current profile from a BMW 3 series prototype car, which is equipped with measurement instrumentation. By tapping the according CAN bus ECU signals, the data from the intelligent battery sensor and important controlled variables in the software module were logged. Note that the micro-hybrid software maturity level was not yet equivalent to today's series cars in the field. The *U*/*I*-profile meets several issues corresponding to the fundamental idea of recuperation in a Micro-HEV: The software mode during the 28 min driving pattern is mainly in the 'charge sustainment' status (see Fig. 4). The frequency of switching to the 'recuperative charging' status was homogeneously spread and the total number of regenerative braking phases resulted in a SOC increase of the mounted battery at moderate temperatures (about 15 °C). At that time, this was a 90 Ah AGM battery comparable to the tested battery types. It was in ordinary use for about 2 months before the profile was logged.

The driving profile was implemented in the BTS-600 test bench software by cutting single sections according to the BER software states. Regenerative braking phases were converted to *U*-charging sections with 14.8 V, charge sustainment phases were converted to *I*-charging sections (CC-charging with $I = 0$ A), discharge phases due to electric consumers were converted to *I*-discharging sections with the according CC. Conventional charging phases, converted to *U*-charging with the according CV, were neglectable. Any ramps were idealized to linearly interpolated or rectangular shape. The resulting *U*/*I*-test bench profile is shown in Fig. 6a (limited to ±50 A). In the lower illustration (Fig. 6b) the corresponding SOC of a test battery starting at 80% SOC is given. The SOC increases due to regenerative charging phases (and sufficient charge acceptance of the battery) and reaches the upper SOC_{max} level defined as 83% in the lab simulation (cf. Fig. 4). At that point the 'active discharge' regime sets in. For practical reasons this regime is not part of the selected driving profile as both the beginning of active discharge and the duration of active discharge (3% C_{20}) are individual for the tested battery at a definite time. Thus, active discharge is simulated in the lab by just eliminating any charge current that would occur in the driving profile after reaching SOC_{max} (left dotted line in Fig. 6). The delivered electrical battery power is balanced with the previously regenerated braking energy, which is the fundamental idea of brake energy regeneration. This approach exactly meets real conditions except for regenerative braking phases, which are accomplished also in the active discharge regime in the BER software.

Once the lower SOC_{min} level is reached again, the lab program switches back to the actual *U*/*I*-profile (right dotted line in Fig. 6). By stringing the whole *U*/*I*-profile consecutively, the typical PSOC curve in Fig. 6b is obtained. The entire investigation is scaled by units of full cycles. The cumulated amount of discharge in Fig. 6b equals the nominal battery capacity for one full cycle.

4.2. Evaluation of charge acceptance

As already mentioned, charge acceptance is a key parameter of a Micro-HEV and of the presented lab investigation. With the described test procedure the charge acceptance of the battery can be evaluated consistently as sketched in Fig. 7.

The PSOC range in the lab simulation is chosen as $SOC_{min} = 80\%$ and $SOC_{max} = 83\%$. At the beginning of each full cycle the battery is conditioned to 80% SOC (related to the latest measured C_{20}) followed by an 8 h break. For every single full cycle the time of occurrence of the first active discharge (t_{FAD}) is an important parameter in the following. It is shaded dark grey in Figs. 6b and 7 and marks the timescale when the active discharge regime sets in for the first time. Thus, the time of occurrence of FAD represents a reliable inverse scale (given as pointer length) for the charge acceptance of the battery in terms of regenerative braking. This is due to the fact that exclusively recuperative charging causes the SOC increase. As indicated in Fig. 7, the effect of the refresh function (performed every 6 full cycles) on the charge acceptance can be investigated by monitoring t_{FAD} for each full cycle.

4.3. Description of the test procedure

In Fig. 8 the time of occurrence of first active discharge, t_{FAD}, is shown versus the number of full cycles. The full cycles are applied in a characteristic scheme: Six full cycles are aggregated to one full

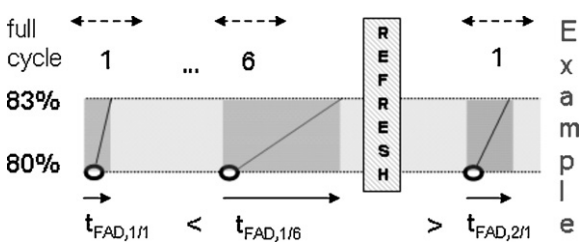

Fig. 7. The time of occurrence of first active discharge (t_{FAD}, shaded dark grey) is sketched as pointer length across the PSOC range. Charge acceptance is inversely scalable by t_{FAD}.

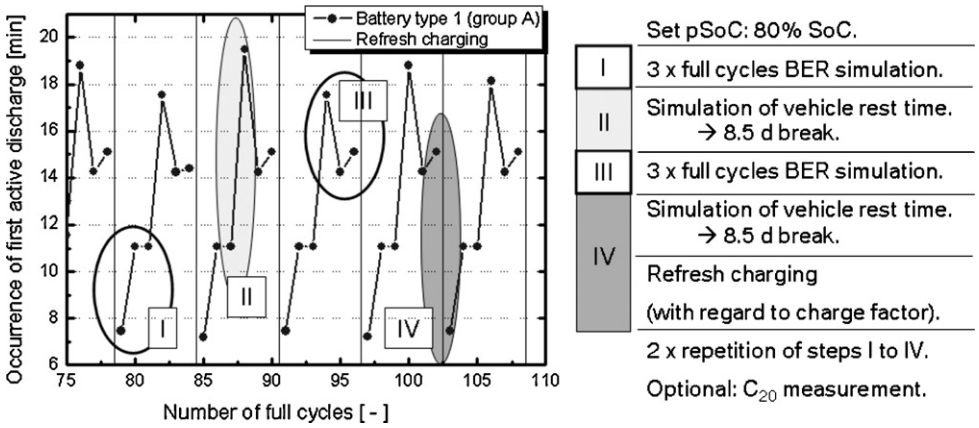

Fig. 8. The test procedure including rest times and battery refresh (steps I–IV) results in a characteristic charge acceptance behavior measured by t_{FAD}.

cycle block indicated by the straight data lines in Fig. 8. At the beginning, a full cycle block consists of three sequenced full cycles, each starting at 80% SOC with an 8 h break in between (see I). By performing each of these full cycles non-stop, the testing is accelerated in order to achieve results within acceptable time—to the disadvantage of perfect realistic conditions, of course. This simplification is, according to Fig. 5a, equivalent to continuously driving more than 500 km per ride.

As a consequence, the investigation would not include any effects induced by a short trip driver and/or long vehicle rest times. However, it is known from field experience that partially discharged batteries operated with frequent and extensive rest times reveal an increased probability of an early failure. Therefore, after three full cycles a vehicle standstill of 200 h (~8.5 days) is attached (see II). By this means, the impact of rest time on charge acceptance can be considered. During the standstill a vehicle quiescent current of 20 mA due to bus and control unit standby (including battery self-discharge current) is simulated. This negative charge balance of 4 Ah is recharged in the fourth full cycle of each full cycle block. For reasons of comparability this charge time does not contribute to t_{FAD} of the fourth full cycle.

Analogous to the three full cycles before the rest time, three additional full cycles of BER simulation are performed after the standstill (see III). The last full cycle is repeatedly followed by 8.5 days rest time with subsequent refresh charging of the battery (see IV). The battery refresh finalizes a full cycle block and is indicated as straight vertical line in Fig. 8. The battery refresh function is also based on a logged driving profile of the prototype car and transferred to the test bench software analogous to the BER simulation profile described in Section 4.1. We remind that refresh charging is based on conventional battery charging with raised charging voltage of 14.8 V. Battery refresh is terminated after recharging the charge deficiency of 20% SOC. Additionally, the battery charge factor is considered by monitoring the final charge current, which has to drop below 500 mA. As a result, battery refresh takes variable time periods.

The PSOC lab simulation is scheduled in four groups each including one exemplar out of two battery types. The groups are described in Table 1. They differ in temperature (controlled in a water bath for all measurements) and the way of applying the refresh function and intermediate capacity measurements. For example, every third full cycle block, i.e. every 18th full cycle, is optionally followed by a C_{20} measurement. The C_{20} acts as SOC scale for the subsequent full cycle blocks. The groups B and D comprise both refresh and C_{20} and differ solely in temperature. The groups A and C act as reference groups as either the battery refresh or the C_{20} is skipped at 25 °C. In order to keep comparability, the PSOC range amplitude is kept at 3%

Table 1
Parameter variation of the lab investigation.

Group	Temperature	Refresh function	C_{20} measurement
A	25 °C	Every 6 full cycles	–
B	25 °C	Every 6 full cycles	Every 18 full cycles
C	25 °C	–	Every 18 full cycles
D	3 °C	Every 6 full cycles	Every 18 full cycles

of the nominal capacity in the course of the lab investigation. This results in an effective relative broadening of the spectrum if capacity loss occurs in the course of the procedure. Thus, evaluation of charge acceptance is related to a fix amount of charge (2.7 Ah).

5. Results and discussion

The introduced test procedure has been performed for 18 months and reached about 100 full cycles for each battery. Transferred to average field conditions this would result in an average mileage of about 65,000 km (cf. Section 3.1), which justifies declaring the investigation as long-termed. Although the test procedure is based on a realistic (not idealized) driving pattern, quantitative analysis of the results is possible at least on a relative scale as the presented testing is subject to defined conditions. Moreover, the driving profile was selected to be representative, but preferably homogeneous (cf. Section 4.1). Thus, interpretation of the results depends essentially on pure battery behavior instead of implications of an extremely chosen driving pattern. Basically, such imprinted effects frequently query the portability of lab based test procedures to the customer. On the other hand, vehicle based field tests satisfy the demand for reference to reality—but mostly not better than phenomenological. Therefore, it was called for both durability lab tests and performance lab tests in literature, e.g. [7], that attempt to meet realistic field-oriented conditions and that are preferably expressive. Our introduced lab investigation is designed to come up to both aspects. In this section, first selected results are presented, beginning with battery refresh efficiency and charge acceptance. Then, voltage behavior over cycling in conjunction with capacity loss and temperature impact is considered.

5.1. Efficiency of battery refresh

In Fig. 8 serious influence of the rest period of 8.5 days (see II) is observed. The time of occurrence of first active discharge, t_{FAD}, is significantly prolonged, from about 11 min to 19.5 min. This increase of 77% is also observed if exclusively the recuperative charging times in the U/I-profile are analyzed until FAD occurs. In

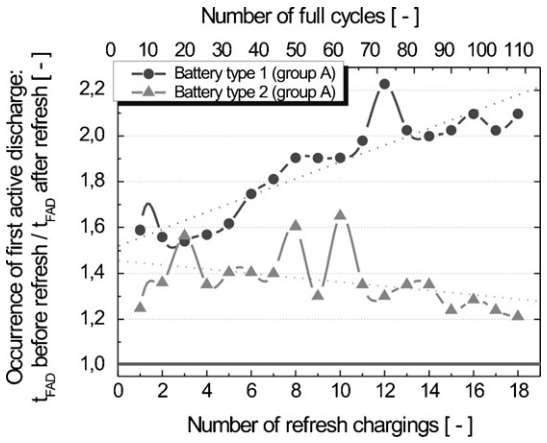

Fig. 9. The effect of battery refresh on charge acceptance can be illustrated as ratio of t_{FAD} before and after the refresh.

particular, by elimination of the interim discharging phases in the *U*/*I*-profile, the potential of 14.8 V is applied for about 6.5 min minutes until time of FAD occurs before the rest time–versus 11.1 min for the full cycle directly after the standstill (see II). Therefore, the net charging time increases for about 75%. As intended by the selection of the driving pattern, this approximate consistency of 77% vs. 75% (maximum accepted error ±5%) allows us to evaluate the simulation profile in total without having to split it up into the single charging/discharging sections afterwards.

This simplified method of analysis is realized in Fig. 9, showing the t_{FAD} ratio of the full cycle before and the full cycle after applying the battery refresh (see IV in Fig. 8). Note that the refresh function is preceded by an 8.5 days rest time period as it is highlighted by area II in Fig. 8. As a consequence we observe a great influence of the battery refresh on the charge acceptance in Fig. 8 (battery type 1, group A). Starting from $t_{FAD} \approx 15$ min before the refresh we would assume $t_{FAD} \approx 27$ min after the rest time. Instead, we observe $t_{FAD} \approx 7.5$ min after the refresh inclusive the preceded rest time. With the previous statements we conclude that battery refresh improves the dynamic charge acceptance by a factor of 3.5, at least under the chosen conditions and on the short-time scale.

The ratio in Fig. 9 is depicted as a function of the number of refresh chargings and the number of full cycles, respectively. For both battery types (group A in Table 1) the ratio is larger than 1 as indicated by the bold gridline. As a consequence, the battery refresh compensates not only the negative effects of the rest time, but absolutely improves the charge acceptance in our test. Out of the automotive point of view this is an important conclusion since the customer value of brake energy regeneration is positively influenceable by on-board energy management for up to more than 100 full cycles. Additionally, battery refresh effectively acts against the assumed increasing customer risk for an early battery failure [16] due to hard sulfation as discussed in Section 3.3.

In spite of that, the two battery types reveal clearly different behavior in Fig. 9. Battery refresh seems to be more effective for the type 1 battery from the beginning of the investigation. With increasing number of full cycles the positive effect of battery refresh is clearly pronounced while the opposite trend is observed for battery type 2 (indicated by the dotted linear fits). In contrast, the range of t_{FAD} is comparable on the absolute scale for both battery types and remains nearly constant over cycling. Merely, the presented splitting characteristics due to battery refresh in Fig. 8 (see IV) changes. For those reasons the phenomenon in Fig. 9 is not explainable by the charge acceptance of battery type 2 getting worse in total, but by some other effect which is not yet fully understood.

5.2. Minimum voltage behavior

In order to discuss the specific influences of the groups A, B and C, one parameter has to be observed that is shared by all groups. We chose the absolute minimum voltage appearing in each full cycle. In a Micro-HEV the voltage minima, measured by the intelligent battery sensor, act as control parameters in the power management especially in terms of power system stability and availability of the auto-start-stop function. Although the test procedure does not include any automatic engine stops and starts, the measured voltage drop due to the simulated electrical consumers still represents the trend of the internal resistance under PSOC operation.

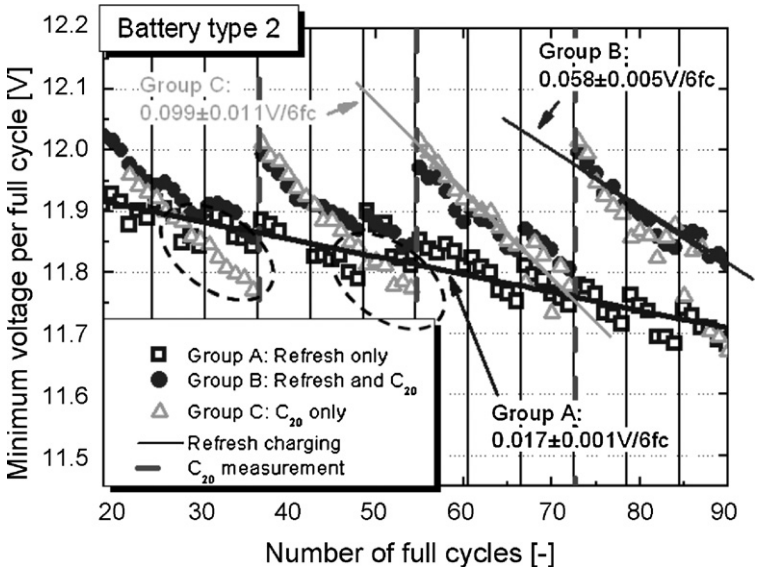

Fig. 10. The minimum voltage gradient of type 2 batteries in groups A, B and C is compared. The linear fit curves illustrate the impact of battery refresh vs. C_{20} (inclusive recharging).

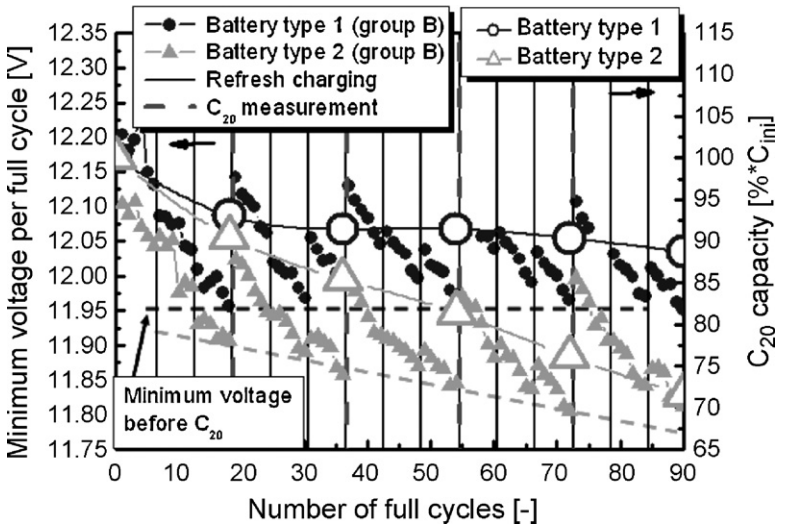

Fig. 11. Analogy of capacity loss and minimum voltage behavior is observed for both battery types.

The minimum voltage per full cycle is depicted in Fig. 10 for battery type 2, the groups A, B and C (all 25 °C) is compared. Battery refresh is indicated as vertical dark line, which does not affect group C. The C_{20} measurement does not affect group A (vertical dashed line). Thus, the influence of both the C_{20} measurement (reflecting the lab influence) and the impact of the refresh function (reflecting the customer situation) can be investigated separately from each other by analyzing groups A and C in Fig. 10. Note that the C_{20} is followed by IU-charging for 24 h at 14.3 V and 25 °C. The higher 14.8 V level is applied exclusively during regenerative braking phases and the battery refresh, respectively. It has to be considered that both elevated voltage and temperature support the dissolution of sulfate crystals, e.g. [7,16]. Thus, the influence of the lab specific recharging is kept as minor as possible.

In spite of that, the C_{20} with subsequent charging can be interpreted as a kind of 'battery reset': The minimum voltage per full cycle is comparable to the initial values even after 80 full cycles—at least at the beginning of a full cycle block. However, this recovery process is observed as only short-lived as the voltage decreases with about 0.1 V per full cycle block. This is given by the section-limited linear fit curve of group C in Fig. 10. The analogous curve fit of group A (none C_{20}) with a slope of about 0.02 V per six full cycles is depressed by a factor of 5. Again, this demonstrates the utility of the battery refresh in a Micro-HEV. Since voltage degradation after simply fully IU-charging the battery with 14.3 V is much more pronounced, the minimum voltage of a group C battery may drop below the voltage of a group A battery near the end of a full cycle block. This effect is indicated by the dashed circles in Fig. 10. However, we point out that the described observation seems to decline over cycling. Therefore, repeated C_{20} measurements might stand for a more positive effect in the long-term than the battery refresh. Of course, we keep in mind that a C_{20} measurement including recharging acts as serious artificial intervention into the on-going battery behavior and is not feasible in the car, anyway.

Nevertheless, the capacity is one of the most common and meaningful parameters in battery testing. As a consequence, further discussion will focus on group B and group D batteries with refresh charging and C_{20} measurements. As expected, the group B battery in Fig. 10 reveals a reduced voltage decrease (of about 0.06 V per full cycle block) compared to group C. This is because the refresh function attenuates the voltage loss starting from the elevated voltage level due to the C_{20} measurement.

5.3. Capacity loss and temperature impact

By means of groups B and D, the observed capacity loss during the Micro-HEV lab investigation is discussed in the last section. Linked to capacity loss, the minimum voltage behavior is illustrated in Fig. 11 for both battery types of group B at first.

The minimum voltage of battery type 2 reveals a voltage drift induced by cycling compared to battery type 1: As highlighted by the dotted lines, the minimum voltage of the last full cycle in advance of a C_{20} is nearly constant up to 90 full cycles (battery type 1). In contrast, this voltage value shows a linear decline of about 0.1 V in the same range in the case of battery 2.

On the right *Y* axis in Fig. 11 the corresponding capacity trend is depicted. Capacity loss accompanies the discussed minimum voltage trend. The type 1 battery preserves capacity after an initial capacity loss of about 10% in good approximation. Instead, battery type 2 undergoes a linear capacity loss of about 30% within 90 full cycles. However, even in case of battery type 2, the detected progress of capacity loss – corresponding to about 4 years cycle life – may still be considered as moderate. In contrast, rather rapid capacity loss due to negative plate sulfation is reported from high-rate PSOC applications in 42 V electrical systems [11]. Further it has to be mentioned, that sulfation progress at the negative plate may be caused by different mechanisms in vehicles that are equipped with ASSF *and* BER compared to those equipped solely with BER. In a high-rate PSOC investigation by Lam et al. [17] it was found that – in contrast to low-rate operation – mainly the negative plate surface is accumulated by sulfate crystals resulting in loss of electroactive surface area.

The described capacity trend in Fig. 11 is not yet fully set in conjunction with the differing behavior of the two battery types concerning refresh efficiency in Fig. 9. As additional parameter for interpretation, temperature is available according to Table 1. The group D batteries complete the measurement matrix at lower temperature (3 °C). They are shown by the use of framed symbols in Fig. 12. Note that the C_{20} measurement and the attached IU-charging are performed at 25 °C. Instead, the complete remaining test procedure is performed at 3 °C, especially the battery refresh function. The capacity splitting between the different battery types at 25 °C is significantly smaller in the case of 3 °C after 90 full cycles. The delta shrinks to remaining 5% relative difference of lost capacity. Interestingly, battery type 2 at 3 °C conserves capacity following an initial capacity loss. In contrast, for battery type 1 the capacity

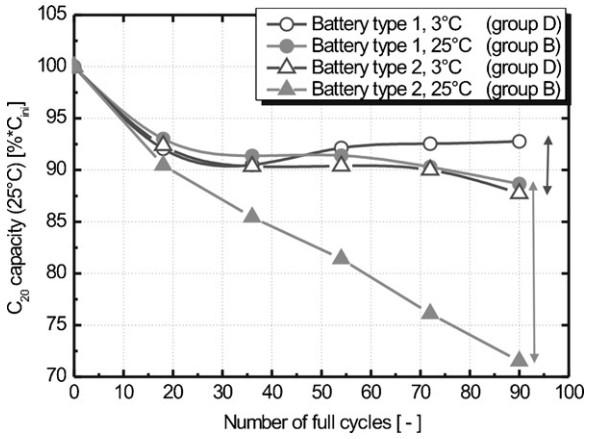

Fig. 12. The temperature influence on the capacity loss is indicated by the length of the arrows after 90 full cycles.

loss in the first 30–40 full cycles even turns into slight regaining of capacity, which lasts at least up to 90 full cycles.

This dependence demonstrates that temperature has a massive influence on the capacity behavior in the accomplished lab simulation. The increased capacity loss observed at 25 °C suggests hard sulfation as major cause. According to Arrhenius' law Pb sulfate crystal growth is strongly favored at elevated temperatures [18]. In our experiment, this effect might compensate the beneficial influence of both temperature and voltage during periodical refreshing. According investigations are nicely demonstrated by Sauer et al. [7]. The colder batteries in group D take advantage of a second effect: Since charge acceptance is worse at lower temperature, the duration of battery refresh is prolonged by a factor of 4 for both battery types in group D compared to group B. As a consequence the elevated charge voltage of 14.8 V is applied significantly longer with respect to the refresh termination criteria. In combination with the depressed Pb sulfate crystal growth rate at 3 °C, the less pronounced capacity loss of both battery types at 3 °C seems to be consistently explainable.

However, the presented discussion does not hold the fact that charge acceptance, introduced as inverse of t_{FAD}, does not significantly decrease over cycling for both battery types at 25 °C. This would be reflected by an increasing offset of t_{FAD} over cycling, which is so far not observed during our test procedure. As a result we interpret that the applied refresh function enables to preserve the ability of charge acceptance unlike capacity in the case of battery type 2 at 25 °C. This phenomenon is not yet fully understood as hard sulfation is usually described as linkage between capacity loss and bad charge acceptance in literature.

In this context various fundamental design parameters of the used battery types have additionally to be taken into consideration. Concerning charge acceptance and sulfation tendency those parameters are the initial acid specific gravity, the initial saturation level of the battery, the ratio of positive active and negative active mass including the exact mass formulae (e.g. additives or expander materials) and the total ratio of delivered acid and active masses. Additionally, critical design parameters of the production process might influence the observed behavior, e.g. formation programs, plate group pressure and porosity of the formed active material. Against the background of this complexity an overall comprehensive explanation of the observations may only be given after tear-down-analysis of the batteries.

6. Summary and outlook

Introductory, the BMW micro-hybrid functions BER and ASSF were described. The emerging challenges for the battery were discussed by means of first field experience. The field data, acquired by the method of after sales analysis, revealed higher cycling rates and lowered SOC distribution on average. Under those conditions and due to the fact that maximum charge acceptance is required for regenerative braking, VRLA batteries in AGM technology promise best performance on request of package and price. Since battery behavior with a PSOC operation strategy in high-volume series applications is widely unknown, we designed a long-term lab investigation under preferably realistic and controllable conditions. We conclude that AGM batteries of both measured types are suitable for the use at least in mid-sized Micro-HEVs. Especially, we demonstrated that periodically recharging of the battery improves charge acceptance significantly. This battery refresh prevents Pb sulfate crystals to grow irreversibly especially in the negative plate as intensely discussed in literature. The maximum capacity loss would account for 30% after 90 full cycles (i.e. about 60,000 km mileage or 4 years) at an average temperature of 25 °C. Note, that the C_{20} measurement plus recharging recovers the battery to some extent as well. The stage of development of the tested batteries was at the beginning of the year 2006.

By continuation of the presented lab simulation we expect an amplification of the observed effects with increasing number of full cycles. At the end of the PSOC simulation we aim for a more complete understanding of the occurring processes in the batteries by performing a profound tear-down-analysis of the tested batteries. Thus, the main present aging processes might be estimated and compared by means of physicochemical analysis. In parallel, we work on an upgrade of the measurement matrix and an even more realistic, i.e. not accelerated, bench test with short ride effects included. This test will serve as link to the verification and validation testing with prototype cars and the field data experience, respectively.

Based on current field experience, there is not yet definitely reliable information on battery failure rates in Micro-HEVs since the maximum age of the according batteries accounts for maximum 15 months at the time of paper submission. However, so far, failure rate analysis does not give any hints for an increased rate compared to conventional cars. Therefore, we conclude that the described operation strategy in combination with the AGM battery technology serves as solid base for the development of advanced Micro-HEVs.

Acknowledgements

We gratefully thank N. Roettger and the colleagues at BMW energy storage division and power supply division for support.

References

[1] C. Diegelmann, J. Stauber, M. Hafkemeyer, S. Wolff, Proceedings of the 7th International Advanced Automotive Battery Conference, Long Beach, May, 2007.
[2] E. Karden, S. Ploumen, B. Fricke, T. Miller, K. Snyder, Journal of Power Sources 168 (2007) 2–11.
[3] S. Wolff, D. Abendroth, W. Weigl, C.-P. Linner, R. Neudecker, M. Schneider, W. Huber, A. Rau, Proceedings of the 7th Stuttgart International Symposium Automotive and Engine Technology, Stuttgart, Germany, March, 2007.
[4] M. Hafkemeyer, F. El-Dwaik, A. Heim, J. Liebl, J. Stauber, F. Traub, Proceedings of the 12th International Conference on Electronic Systems for Vehicles, Baden-Baden, October 6–7, 2005.
[5] M. Schmid, M. Schöllmann (Eds.), Elektrisches Energiemanagement: iGR, ein Weg zu BMW EfficientDynamics (Electrical Energy Management: iGR, A Way Towards BMW EfficientDynamics), Haus der Technik Fachbuch, Germany, 2007; U. Brill (Ed.), Energiemanagement und Bordnetze II (Energy Management and Power Supplies II), expert verlag, Germany, 2007.

[6] E. Karden, S. Ploumen, E. Spijker, D. Kok, D. Kees, P. Phlips, Energiemanagement und Bordnetze (Energy Management and Power Supplies), Haus der Technik Fachbuch, expert verlag, Germany, 2004.
[7] D.U. Sauer, E. Karden, B. Fricke, H. Blanke, M. Thele, O. Bohlen, J. Schiffer, J.B. Gerschler, R. Kaiser, Journal of Power Sources 168 (2007) 22–30.
[8] U.M. Fayyad, G. Piatetsky-Shapiro, P. Smyth, R. Uthurusamy, Advances in Knowledge Discovery and Data Mining, MIT Press, 1996.
[9] G. Piatetsky-Shapiro, W.J. Frawley, Knowledge Discovery in Databases, MIT Press, 1992.
[10] E. Karden, P. Shinn, P. Bostock, J. Cunningham, E. Schoultz, D. Kok, Journal of Power Sources 144 (2005) 505–512.
[11] P.T. Moseley, Journal of Power Sources 127 (2004) 27–32.
[12] P. Ruetschi, Journal of Power Sources 127 (2004) 33–44.
[13] T. Handschuh, Untersuchung des Betriebs- und Alterungsverhaltens von Blei-Säure-Akkumulatoren bei für Hybridantriebssysteme typischen Belastungen, Ph.D. Thesis, University of Ulm, 2007.
[14] I.K. Gibson, K. Peters, Journal of Power Sources 8 (1982) 143–157.
[15] M. Thele, E. Karden, E. Surewaard, D.U. Sauer, Journal of Power Sources 158 (2006) 953–963.
[16] H.A. Catherino, F.F. Feres, F. Trinidad, Journal of Power Sources 129 (2004) 113–120.
[17] L.T. Lam, N.P. Haigh, C.G. Phyland, A.J. Urban, Journal of Power Sources 133 (2004) 126–134.
[18] D. Berndt, Maintenance-free Batteries: Lead-acid, Nickel/Cadmium, Nickel/Hydride: A Handbook of Battery Technology, Research Studies Press Ltd., Taunton, Somerset, England, 1993.